The Journal of Experimental Biology 212, 3148-3155
Published by The Company of Biologists 2009
doi:10.1242/jeb.033373

Wetting properties on nanostructured surfaces of cicada wings

Mingxia Sun[1,2], Gregory S. Watson[3], Yongmei Zheng[4], Jolanta A. Watson[3] and Aiping Liang[1,*]

[1]Key Laboratory of Zoological Systematics and Evolution, Institute of Zoology, Chinese Academy of Sciences, Beijing 100101, China, [2]Graduate School of Chinese Academy of Sciences, Beijing 100039, China, [3]School of Pharmacy and Molecular Sciences, James Cook University, Townsville, QLD 4811, Australia and [4]School of Chemistry and Environment, Beijing University of Aeronautics and Astronautics, Beijing 100191, China

*Author for correspondence (liangap@ioz.ac.cn)

Accepted 29 June 2009

SUMMARY

This study has investigated the wettability of forewings of 15 species of cicadas, with distinctly different wetting properties related to their nanostructures. The wing surfaces exhibited hydrophilic or weak to strong hydrophobic properties with contact angles ranging from 76.8 deg. to 146.0 deg. The nanostructures (protrusions), observed using environmental scanning electron microscopy (ESEM), were classified into four types according to the patterning, diameter (82–148 nm), spacing (44–117 nm) and height (159–446 nm). Surface analysis by X-ray photoelectron spectroscopy (XPS) showed significant differences in wing membrane chemistry. Thus, wetting properties at the macroscopic scale were dependent on slight differences in nanoscale architecture and composition of the wax layer. This investigation offers insights into the diversity of nanostructuring and how subtle small-scale changes may facilitate large changes in wettability.

Supplementary material available online at http://jeb.biologists.org/cgi/content/full/212/19/3148/DC1

Key words: cicada, forewing, nanostructure, chemistry, hydrophobicity.

INTRODUCTION

Biological surfaces have variable wetting properties because of their fine nanostructures and have attracted the interest of biologists and biomimetic researchers (Jiang et al., 2004; Xie et al., 2004; Shi et al., 2005; Ming et al., 2005; Zhang et al., 2006). Of notoriety is the lotus plant, the leaves of which has superhydrophobic surfaces and are self-cleaning (Barthlott and Neinhuis, 1997; Neinhuis and Barthlott, 1997). This is a result of the rolling motion of water droplets collecting surface dust resting on micro-papillae and nano-scale branchlike structures. Many insects have non-wetting surfaces to contend with the risks associated with living in an environment which offers little protection against wetting by rain and other sources of water that the insect may encounter. The water strider for example (Gao and Jiang, 2004; Feng et al., 2007) can stand and walk on water owing to nanogroove structures of microsetae as well as wax on the legs aiding in water repellency. Butterflies, by contrast, have a high wing area to body mass ratio and additional weight from contamination (water and/or particulates) can potentially have a detrimental effect on the flight capabilities of these insects. The superhydrophobic property of their wings is a consequence of the combination of micro- and nanostructures on the wing scales (Cong et al., 2004; Fang et al., 2007). Cassie and Baxter (Cassie and Baxter, 1944) formulated a theory regarding the unwettability of surfaces, demonstrating a quantitative relationship between wettability and wing sub-structure size (e.g. radius of the ridges on wing) and spacing (distance between ridges).

The cicadas, with about 2500 known species, constitute a distinct group of phytophagous insects within the Hemiptera. The individuals are typically 20–50 mm long with transparent, well-veined, membranous wings. The putative function(s) and functional efficiencies of periodic nano-structures on the surface of cicada wings have been investigated by atomic force microscopy (Watson et al., 2008). Particle adhesion data showed the wings represent a low surface energy membrane with anti-wetting properties. The wings also have been shown to have antireflection (Stoddart et al., 2006; Watson et al., 2008) and strong mechanical properties (Song et al., 2004; Watson et al., 2008). The non-wetting property of cicada wings has been attributed to nanostructuring, comprising protrusions typically in the sub-micron range in height and spacing (Wagner et al., 1996; Barthlott and Neinhuis, 1997; Sun et al., 2005; Feng and Jiang, 2006; Watson et al., 2008). Indeed biomimetic-structured surfaces similar to cicada nanostructure arrays have been shown to have anti-wetting properties (Zhang et al., 2006). These studies have prompted us to investigate wettability of cicada wings, relating microstructure dimensions (e.g. depth) and chemistry.

Fifteen species of cicadas were studied to investigate the wetting properties of the forewings. The associated nanostructures were carefully examined and their role in wetting was assessed based on the architecture types, patterning and basic wetting models in order to gain a better understanding of the microstructure-tunable wettability.

MATERIALS AND METHODS

Dried or fresh specimens of 15 cicada species were investigated in this study (Fig. 1). The species studied (with their place and date of collection) were: *Chremistica maculata* (China: Yunnan, 20.v.2002), *Pomponia scitula* (China: Yunnan, 28.v.1995), *Mogannia hebes* (China: Fujian, 3.vi.1955), *Leptopsalta bifuscata* (China: Hebei, 22.viii.1964), *Mogannia conica* (China: Yunnan, 3.v.1957), *Meimuna durga* (China: Yunnan, 28.v.1957), *Aola bindusara* (China: Yunnan, 29.iv.1956), *Meimuna microdon* (China: Hainan, 9.v.2007), *Meimuna mongolica* (China: Beijing, 8.viii.1949), *Platylomia radha* (China: Yunnan, 9.v.1957), *Dundubia vaginata* (China: Yunnan, 13.iv.1956), *Dundubia nagarasingna* (China: Yunnan, 14.v.1957), *Meimuna opalifer* (China: Shaanxi, 23.vii.1998), *Terpnosia vacua* (Japan: Kyoto, 24.v.1932) and

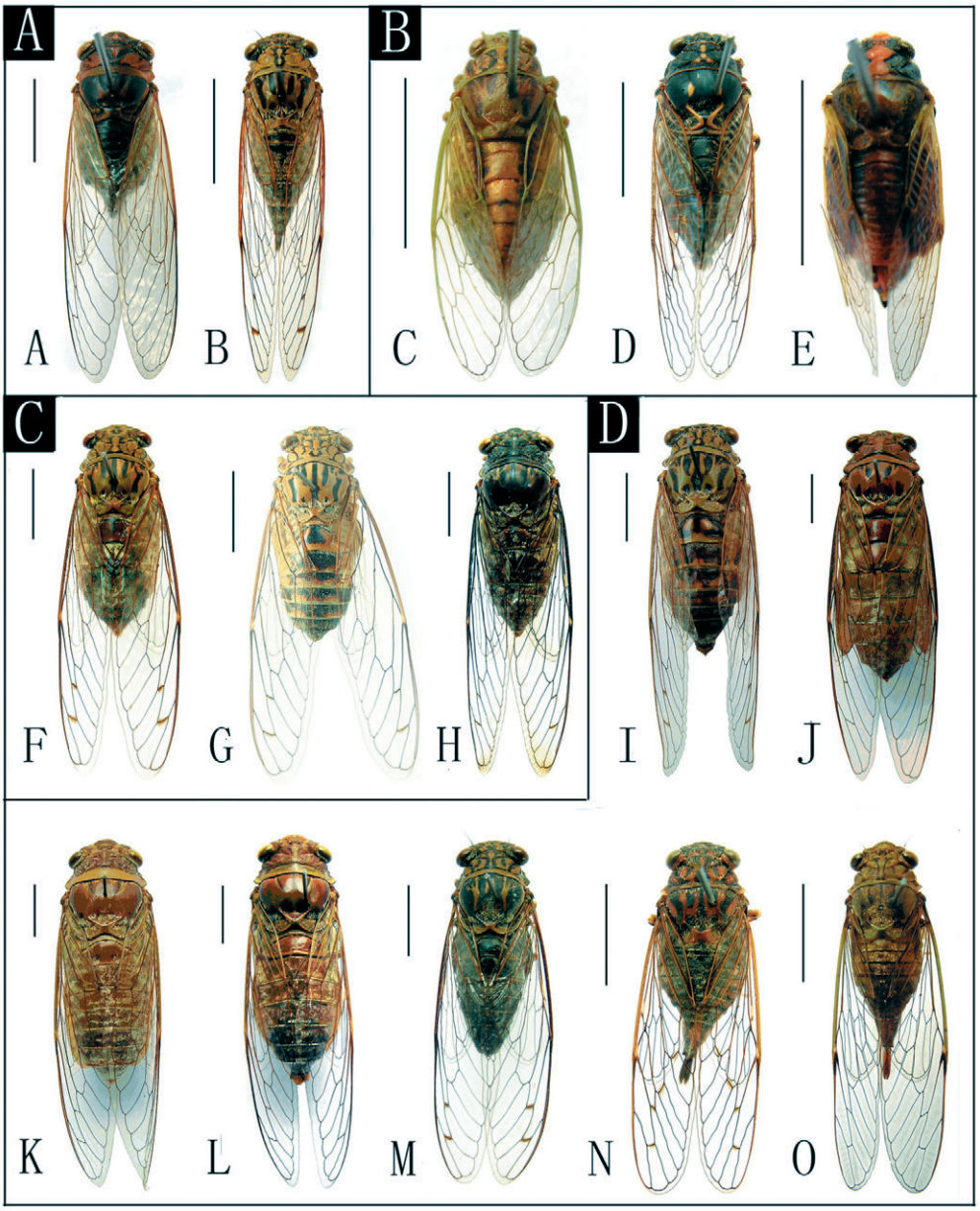

Fig. 1. Adult cicada species used in this study. (A) *Chremistica maculata*; (B) *Pomponia scitula*; (C) *Mogannia hebes*; (D) *Leptopsalta bifuscata*; (E) *Mogannia conica*; (F) *Meimuna durga*; (G) *Aola bindusara*; (H) *Meimuna microdon*; (I) *Meimuna mongolica*; (J) *Platylomia radha*; (K) *Dundubia vaginata*; (L) *Dundubia nagarasingna*; (M) *Meimuna opalifer*; (N) *Terpnosia vacua*; (O) *Terpnosia jinpingensis*. They are grouped according to the type of wing surface. Scale bars, 1 cm.

Terpnosia jinpingensis (China: Hainan, 10.v.2007). The specimens studied were deposited in the Zoological Museum at the Institute of Zoology, Chinese Academy of Sciences, Beijing, China.

Forewings of each cicada species were excised from the insects approximately a third of the way from the wing apex for measurements on the remigium region.

To characterize the wettability of cicada wings, a number of wetting angles were measured; the static contact angle (CA), sliding angle (SA), advancing (θ_A) and receding angles (θ_R) and contact angle hysteresis (defined as the difference between the advancing and receding angles).

The CAs and SAs were measured with an optical contact angle meter (Dataphysics Contact Angle System OCA, Filderstadt, Germany) using the sessile drop method. The wings were fixed on slides with double-sided adhesive. The volume of water droplets was 3 μl for CA measurements (Miwa et al., 2000) and 1~7 μl for SA measurements. The 15 samples were cleaned with flowing deionized water before experiments in order to remove foreign particulates. Five of the species (*C. maculate*, *M. hebes*, *P. scitula*, *M. conica*, *M. mongolica*) underwent additional processing and were cleaned with a general writing brush dipped in deionized water. Each wetting angle was measured at ten different points on each wing, and average values and standard deviations (in brackets) were calculated. The θ_A(s) and θ_R(s) were recorded by adding and removing a small amount of water from the drop, respectively.

For observation of nanostructures (surface protrusions), the wing samples were coated with a thin layer of gold using an ion sputtering instrument (KYKY SBC-12, Beijing, China) and viewed under an environmental scanning electron microscope (Quanta 200 FEG, FEI, Eindhoven, Netherlands). The mean values and standard deviations of diameter (*R*), spacing (*L*) and height (*H*) of protrusions were based on twenty replicates for each species.

The chemical components of the wing surfaces of four species were ascertained using X-ray photoelectron spectroscopy (PHI Quantera SXM, ULVAC-PH INC, Chigasaki, Japan). Four cicada wing samples were fixed onto the stage using conductive adhesive, with the full-spectrum analysis (with the exception of the narrow-band spectrum) examined in two different positions of each sample

(supplementary material Fig. S2). Experimental conditions: monochrome, anode target was Al, the energy resolution was 0.5 eV, sensitivity was 3 M CPS, angle-resolved was 45 deg., X-launched harness was 9 μm–1.5 mm^2, the pressure in the vacuum chamber was 6.7×10^{-8} Pa. Sputtering: Ar^+ gun scan based on an area of 1×1 mm^2, sputtering rate was ca. 14 nm min^{-1}, energy was 2 kV, the emission current was 20 mA, standard sample was thermal oxidation SiO_2/Si.

The wetting state of the rough surfaces was approximated based on two established models: those of Wenzel (Wenzel, 1936) and Cassie (Cassie and Baxter, 1944). The Wenzel model states that liquid may fill into the grooves of the microstructures and then produce 'wetting contact', which determined by $\cos\theta_W=r\cos\theta_0$, where r is the roughness factor (the ratio of actual area to the geometrically projected area of surface), θ_W is the apparent contact angle on a rough surface, and θ_0 is the contact angle on a smooth surface of the same material. The Cassie model is a development of the Wenzel model: $\cos\theta_C=\varphi(1+\cos\theta_0)-1$, where φ is solid fraction in contact with the liquid. Thus, the roughness factor (r) of wing surfaces was calculated (supplementary material Table S1) using the following equation:

$$r = \frac{(R+L)^2 + 4RH}{(R+L)^2} .$$

For the surface having a high contact angle, the fraction (φ) was determined (supplementary material Table S1) using the equation:

$$\varphi = \frac{R^2}{(R+L)^2} ,$$

where R, L and H are the diameter, spacing and height of protrusions, respectively. Given θ_0=105 deg. (Holdgate, 1955), and substituting the values of r and φ into the two model equations, the values of $\cos\theta_W$ and $\cos\theta_C$ were obtained (supplementary material Table S1).

RESULTS

Microstructure observation

Based on the microstructure, the surfaces were classified into four types A, B, C and D (Fig. 2). The protrusions varied in diameter (82–148 nm), spacing (44–117 nm) and height (159–446 nm; Table 1). The type A surfaces are cylindrical with rounded tops, some of which were joined at the apex. The type A surface features of *C. maculata* wings (Fig. 2A) measured, R=97±5 nm (± s.d.), L=92±11 nm, H=309±24 nm. Type 'B' surfaces are cylindrical with rounded tops, which in *M. conica* (Fig. 2B) had the dimensions, R=95±7 nm, L=115±15 nm, H=159±13 nm. The type C surfaces, e.g. *M. microdon*, had the dimensions, R=82±3 nm, L=89±7 nm, H=208±8 nm, appear to be cylindrical or slightly conical with rounded tops but no posts were connected and the spacing between protrusions was similar to or greater than their individual diameters (Fig. 2C). A type D surface was similar to that of type C but the spacing between protrusions was less than their diameters (Fig. 2D), e.g. *T. jinpingensis* with dimensions R=141±5 nm, L=46±4 nm, H=391±24 nm.

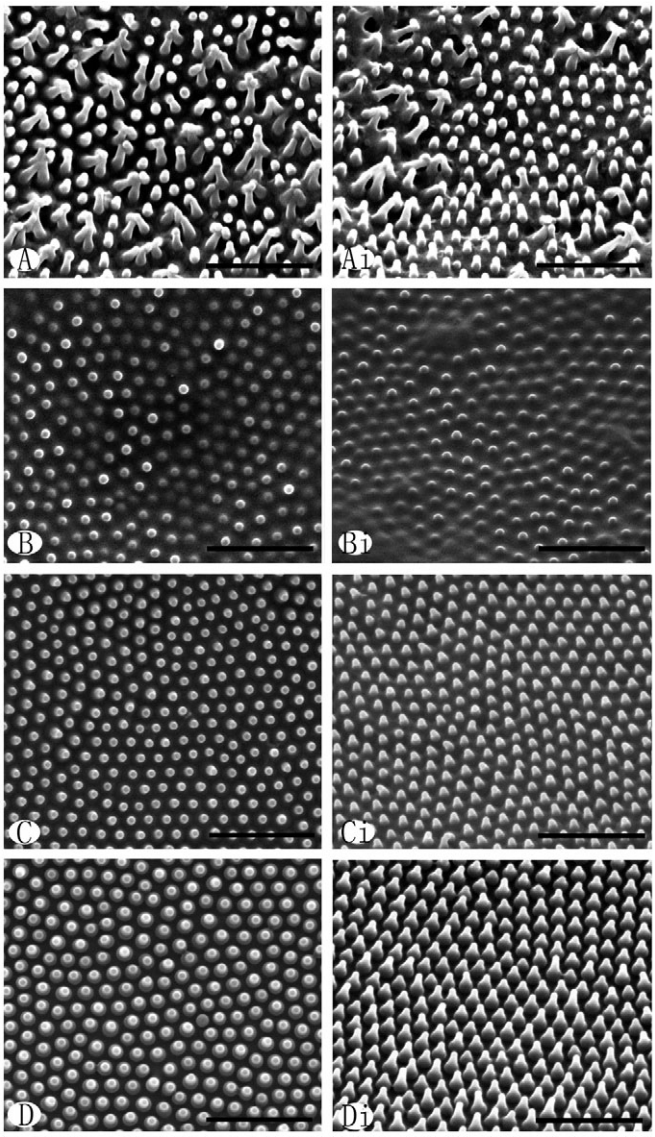

Fig. 2. SEM images of the four types of surfaces of cicada wings. (A) Type A (*C. maculata*); (B) Type B (*M. conica*); (C) Type C (*M. microdon*); (D) Type D (*T. jinpingensis*). The surfaces in Ai, Bi, Ci, Di were titled 30 deg. from those in A, B, C, D, respectively. Scale bars, 1 μm.

Measurements of contact angle, sliding angle, advancing and receding angles

The contact angles (CAs) of water droplets on the wing surfaces of the 15 species of cicadas ranged from 76.8 deg. to 146.0 deg. (Fig. 3; supplementary material Fig. S1). The wing surface of *T. jinpingensis* exhibited the greatest CA of ~146.0 deg. (Table 1). The sliding angles (SAs) of the 12 wing surfaces were high when the volume of the water droplet was less than 3 μl. The water droplets remained on the surface in a state of equilibrium without any lateral movement when the plate was titled 90 deg. When water droplets greater than 3 μl were deposited on type C and D surfaces the droplets had a tendency to roll off at the slightest inclination (2~11 deg.) of the surfaces. Some droplets did, however, retain their hanging postures in response to gravity when the plate was titled 90 deg. (Fig. 3; supplementary material Fig. S1). The CA hysteresis of types C and D (0.7~2.1 deg.) were lower than that of type B (e.g. *M. conica*, 6.2 deg.; supplementary material Table S2) from the measurements of θ_A and θ_R.

X-ray photoelectron spectroscopy analysis of wing surfaces

Chemical properties of the four types of forewing surfaces were analyzed by X-ray photoelectron spectroscopy (XPS). Despite the similar character of the peaks, the binding energies (b.e.) of these surfaces were different (Fig. 4). The binding energies of wing

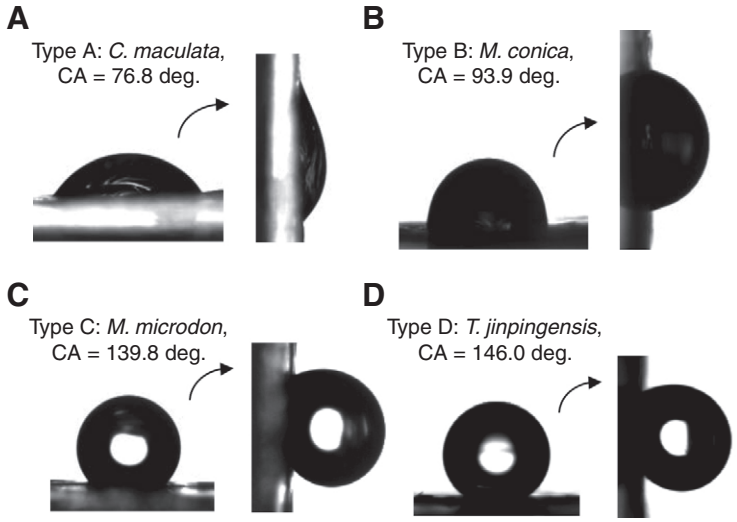

Fig. 3. Optical images of water droplets on the four types (A–D) of wing surfaces examined. (A) *C. maculata*, contact angle (CA)=76.8 deg.; (B) *M. conica*, CA=93.9 deg.; (C) *M. microdon*, CA=139.8 deg.; (D) *T. jinpingensis*, CA=146.0 deg. The right hand image in each pair is shows the plate tilted 90 deg. to that on the left.

surfaces of *C. maculata* and *M. hebes* were found to be greater than those of *M. microdon* and *T. jinpingensis* (supplementary material Fig. S2). The percentages of atom content (a.c.) of the six identified elements (carbon, nitrogen, oxygen, silicon, sulphur and calcium) were different in the four species (Table 2).

As shown in Fig. 4, the strongest characteristic photoelectron peak at ~285 eV showed carbon to be the main component; the highest percentage of carbon was found on the surface of *T. jinpingensis* (92.44) followed by *M. microdon* (81.78), *C. maculate* (81.31) and *M. hebes* (75.21) (Table 2). At the binding energies of ~532 eV, 400 eV and 102 eV, the weak peaks denoted the elements oxygen, nitrogen and silicon, respectively. A small amount of calcium and sulphur (~347 eV and 169 eV, respectively) were also found. *C. maculata* had the highest nitrogen content (1.57), whereas oxygen (18.03) and silicon (6.12) were the most abundant on the surface of *M. hebes*. The surface of *M. microdon* contained sulphur but no elemental calcium (Table 2).

DISCUSSION

Relationship between microstructure and wetting properties

The experimental results revealed that a difference in the general topographical architecture and/or nanostructure dimensions corresponded to differences in the wetting properties. The wettability of forewings can be attributed to the following criteria.

(1) Different configurations of protrusions resulted in a variety of wetting properties. Types A and B surfaces exhibited significantly lower hydrophobicity than types C and D (Table 1). In type A, the protrusions are connected at the apex and the surface patterning is more disordered than in types C and D. This structuring can facilitate a large solid–liquid interface that produces a spreading over the surface (Jin et al., 2005). In type B, the surface consists of single-scale protrusions which are less hydrophobic than the dual scale-structured surfaces of types C and D. This may be due to the hierarchic structures (types C and D) trapping more air under the water droplets (Zhang et al., 2003; Patankar, 2004; Ming et al.,

Table 1. Mean values and standard deviations (in brackets) of wing surface microstructure parameters of 15 cicada species, based on the Wenzel and Cassie models

Type	Species	Diameter (*R*; nm)	Spacing (*L*; nm)	Height (*H*; nm)	CA (deg.)	θ_w (deg.)	θ_c (deg.)
A	*C. maculata*	97 (5)	92 (11)	309 (24)	76.8 (13.9)	–	143.6
	P. scitula	84 (5)	84 (11)	282 (18)	91.9 (5.9)	–	144.6
B	*M. hebes*	85 (7)	95 (11)	164 (8)	78.4 (5.0)	134.7	146.6
	L. bifuscata	90 (5)	117 (13)	200 (52)	81.3 (8.3)	105.0	149.3
	M. conica	95 (7)	115 (15)	159 (13)	93.9 (8.3)	127.7	148.0
C	*M. durga*	89 (5)	89 (9)	257 (24)	134.8 (5.7)	171.4	144.6
	A. bindusara	84 (4)	91 (13)	234 (18)	135.5 (5.2)	157.4	146.0
	M. microdon	82 (3)	89 (7)	208 (8)	139.8 (4.5)	149.6	146.1
D	*M. mongolica*	128 (4)	47 (5)	417 (26)	123.3 (12.7)	–	127.1
	P. radha	137 (5)	44 (3)	288 (12)	136.5 (5.2)	–	125.1
	D. vaginata	132 (6)	56 (7)	363 (22)	141.3 (3.3)	–	129.4
	D. nagarasingna	128 (6)	47 (5)	316 (18)	141.6 (4.5)	–	127.1
	M. opalifer	148 (6)	48 (5)	418 (38)	143.8 (6.0)	–	125.3
	T. vacua	141 (5)	44 (4)	446 (28)	144.2 (6.8)	–	124.7
	T. jinpingensis	141 (5)	46 (4)	391 (24)	146.0 (2.6)	–	125.4

CA, contact angles; θ_W, apparent contact angle on rough surface in the Wenzel model; θ_C, apparent contact angle on rough surface in the Cassie model. Height values were calculated from inclination of the surface by 30 deg.

A dash indicates an inaccessible angle of θ_W because the value of $\cos\theta_W$ is out of the range (–1 to 1) based on the Wenzel model (see supplementary material Table S1).

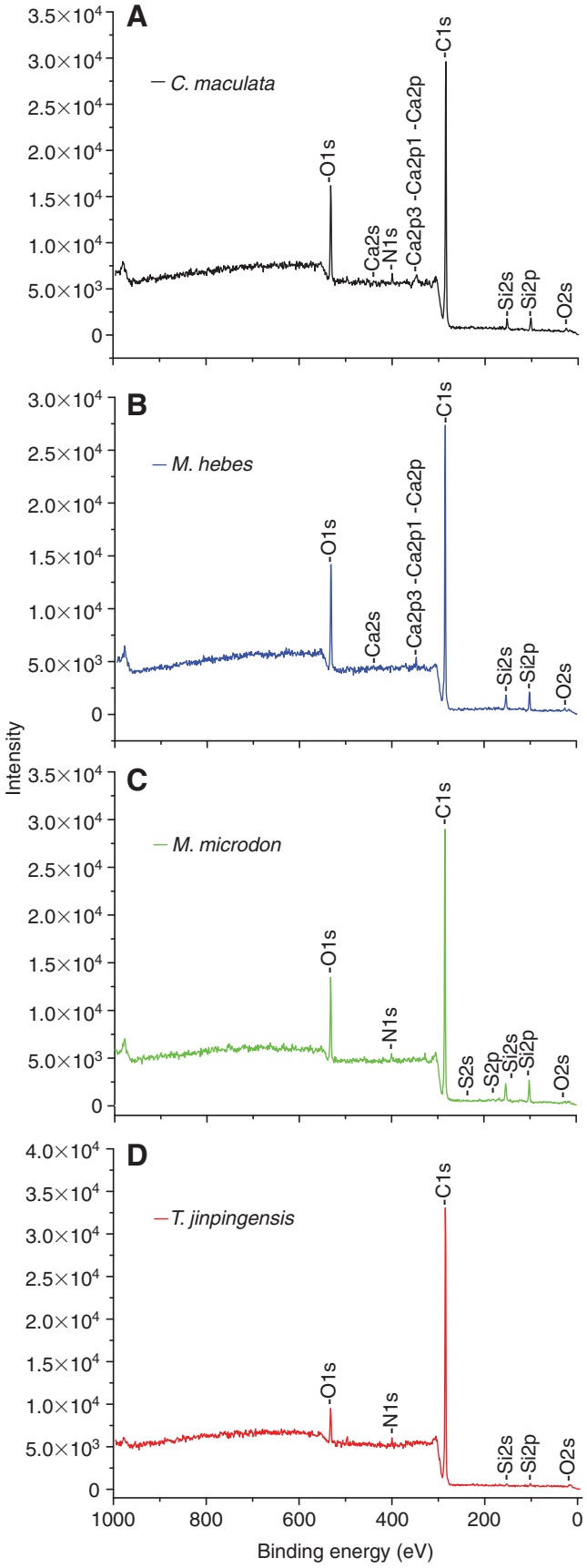

Fig. 4. X-ray photoelectron spectroscopy data of the four types (A–D) of cicada wings. (A) *C. maculata*; (B) *M. hebes*; (C) *M. microdon*; (D) *T. jinpingensis*.

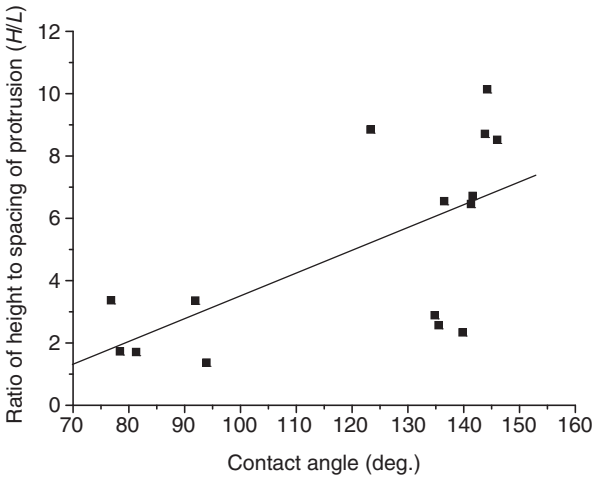

Fig. 5. Plot of the contact angle with the ratio of height (*H*) to spacing (*L*) of the protrusions. Each symbol represents one of the species examined.

2005). Type B structures were typically shorter than those of the other samples or were more variable in height resulting in a more heterogeneous pattern (*L. bifuscata*). In type B samples, the hydrophobicity of the two-dimensionally nanostructured surfaces (e.g. *L. bifuscata* and *M. conica*) can be considered in the context of porous materials with hydrophilicity, where capillary action occurs easily with a rapid accumulation of liquid in the surface structure. Regions on the wing membrane that have short protuberance may facilitate the wetting process. These regions may fill with water first and then partially or completely wet the surface under the water droplet. The smaller solid–liquid contact area can result in a smaller apparent contact angle (Zheng et al., 2004), as in the example of the *L. bifuscata* surface, in which the solid–liquid contact area is less than that of *M. conica* (0.189 and 0.205, respectively) with a smaller contact angle (81.3 deg. and 93.9 deg., respectively). This hydrophilic nature of the surface indicates that the water droplet is in the intermediate state of spreading and imbibition due to hemi-wicking (Bico et al., 2002). The well ordered arrays, as represented by types C and D have stronger hydrophobicity, due in part to their higher roughness factor and the resulting solid–liquid contact area. However, the more heterogeneous and disordered structuring (types A and B) were weakly hydrophobic.

(2) The ratios L/R and H/L are important criteria for determining hydrophobicity (supplementary material Table S1). For types A, B and C, the values of L/R were equal to or close to unity, with H/L in the range of ~1.37 to ~3.37. For the higher hydrophobic surfaces (as type D), the values of L/R ranged between ~0.31 and ~0.42, whereas the values of H/L were 6.46~10.14. This indicated that the L/R ratio had a negative correlation with wettability (Fig. 5), and the H/L ratio had a positive correlation with wettability (Fig. 6). Thus the combined effect of the three parameters (Fig. 7) results in enhanced hydrophobicity.

(3) In accordance with the Wenzel and Cassie models, the roughness factor (r) and the solid fraction (φ) were calculated using Eqns 1 and 2 (supplementary material Table S1). As per the Wenzel model, the hydrophobicity is increased by increasing the roughness factor, however, in line with the Cassie model, it is the reduction of the actual contact area of the solid–liquid that is responsible for increasing the hydrophobicity. The roughness factor for types A, B and C surfaces was found to range between r~2.36 and ~4.37. The

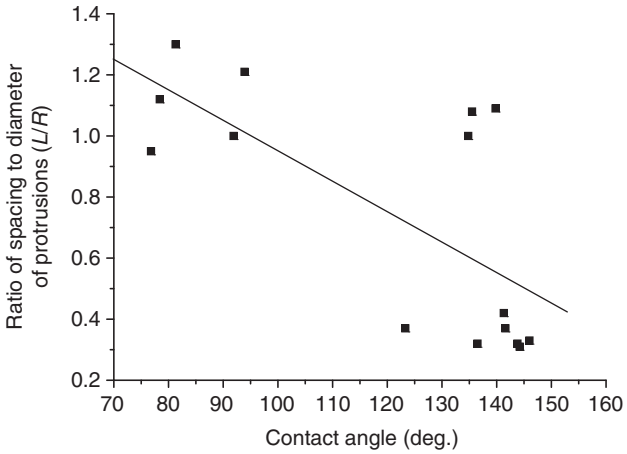

Fig. 6. Plot of the contact angle with the ratio of spacing (*L*) to diameter (*R*) of the protrusions. Each symbol represents one of the species examined.

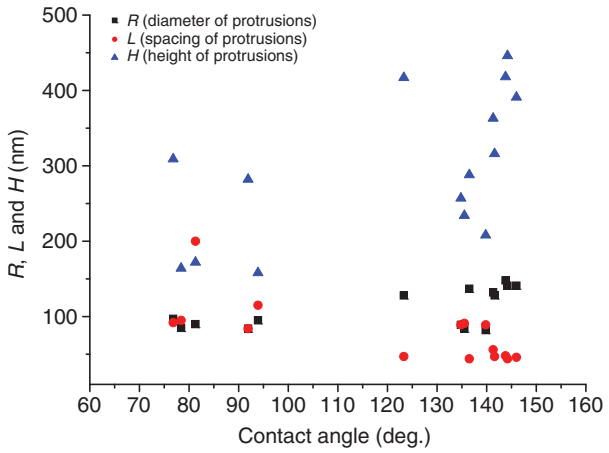

Fig. 7. Relationship of contact angles with diameter, spacing and height of the protrusions. Each symbol represents one of the species examined.

main reason for the different hydrophobicities can be explained as follows. The configurations of protrusions in the hydrophobicity play a determining role where wetting behaviour is influenced by non-homogeneous and disordered structuring in the three dimensions. The applicability of the Wenzel and Cassie–Baxter approximations has in recent times come into question (Nosonovsky, 2007a; Gao and McCarthy, 2007; Panchagnula and Vedantam, 2007; McHale, 2007; Bormashenko, 2008; Goodwyn et al., 2008; Marmur and Bittoun, 2009). Indeed on the surfaces in our study, local conditions at the contact line, and global considerations in relation to the solid–liquid interfacial area may be influenced to varying extents by the surface irregularities. The type D roughness factor ranged from ~5.82 to ~8.35. This is a high roughness factor and indicates strong hydrophobicity. As shown in supplementary material Table S1, only six values of $\cos\theta_W$ were in the range –1 to 1 (–0.704, –0.259, –0.611, –0.989, –0.923, –0.863); thus, water droplets of type D did not conform to either the Wenzel or Cassie state because of their large surface roughness factor (Youngblood and McCarthy, 1999; Lafuma and Quéré, 2003). The solid–liquid contact area of type D was greater than on the other three types of surfaces, which indicated type D was not in the Cassie state, but midway between the Wenzel and Cassie approximations. The type C surfaces should be in a Cassie state as the surfaces with the smaller fraction (φ) of solid–liquid contact area showed higher hydrophobicity (supplementary material Table S1). The measurement of advancing and receding angles showed a higher hysteresis on type B surfaces than on the other sample surfaces (supplementary material Table S2). For types A and B, droplets of 1~7 μl were pinned on the surfaces. Droplets slid a short distance on surface types C and D when titled at a small angle about (2~11 deg.). The droplets then became re-pinned to the surfaces. This also indicated the droplets on types C and D surfaces were not initially in the Wenzel state; when the surfaces were titled, the drops would transform into the Wenzel state and become pinned to the membrane. It is noteworthy that well ordered fabricated nanostructures of similar dimensions to the natural structures examined in our previous study (Watson and Watson, 2004) have shown a good correlation with the Cassie–Baxter and Wenzel

Table 2. List of atom content, binding energy and valence state of elements found on wing surfaces of four cicada species

		Species			
Elements	Parameters	*C. maculata*	*M. hebes*	*M. microdon*	*T. jinpingensis*
C1s	a.c.	81.31	75.21	81.78	92.44
	b.e.	284.7527	284.8166	284.784	284.8467
	v.s.	C-C, C-H	C-C, C-H	C-C, C-H	C-C, C-H
N1s	a.c.	1.57	0.52	0.70	1.26
	b.e.	400.0527	400.4166	399.984	400.1467
	v.s.	N-C	N-C	N-C	N-C
O1s	a.c.	13.37	18.03	11.70	5.67
	b.e.	532.0527	532.4166	532.184	532.3467
	v.s.	O-H, O-S	O-H, O-S	O-H, O-S	O-H, O-S
Si2p	a.c.	3.20	6.12	5.64	0.61
	b.e.	101.9527	102.2166	101.984	101.7467
	v.s.	Si-O, Si-N	Si-O, Si-N	Si-O, Si-N	Si-O, Si-N
Ca2p	a.c.	0.54	0.12	–	0.03
	b.e.	347.4527	347.5166	–	347.3467
	v.s.	Ca-O	Ca-O	–	Ca-O
S2p	a.c.	–	–	0.19	–
	b.e.	–	–	169.2	–
	v.s.	–	–	S-C, S-O	–

a.c., atom content; b.e., binding energy; v.s., valence state.

approximations (Martines et al., 2005). It is worth mentioning that the two classic models may not be fully appropriate or provide a complete description when used to analyse the wettability of biosurfaces for much higher roughness factor values and/or inhomogeneous structuring.

As the above analysis shows, CAs did not depend solely on the diameter, spacing or height of protrusions. These three protrusion parameters partially determine the hydrophobicity of the forewing surfaces. The configurations of protrusions also play a vital role in determining the hydrophobic nature and state of the surfaces.

Relationship between chemistry and wetting properties

Wettability of a solid surface is primarily governed by surface chemistry in combination with the microstructure (Chen et al., 1999; Nakajima et al., 1999; Youngblood and McCarthy, 1999; Öner and McCarthy, 2000; Extrand, 2004; Shiu et al., 2004; Hsieh et al., 2005). An artificial smooth surface can be prepared by materials with very low surface free energy but the resulting CA is no greater than 120 deg. (Nishino et al., 1999).

The epicuticle is the outermost layer of cuticle not containing chitin, and is about 1~3 μm thick. The layers of epicuticle vary depending on the species of insect but generally it contains three layers: the inner cortex layer, mid wax layer and outer cement layer. X-rays can only penetrate to a depth of less than 10 nm where only photoelectrons from the outer atomic layers of the sample surface are detected. So the chemical components detected by X-rays should only be those present in the epicuticle.

The main components of the cement layer are proteins and lipids. In the wax layer, the main components are long-chain hydrocarbons and other lipids and fatty alcohols. The cortex layer is secreted by purple–red cells and is divided into two layers. The inner layer is thick, loose and mainly composed of a lipoprotein and polyphenol complex. The outer layer is thin and compacted, and the nature of the lipoprotein after being quinine-tanned is quite stable. This outer layer is also known as tanned cuticulin, which has a special affinity to the oriented polar group of the wax layer (Chapman, 1998).

Based on the valence states of the elements examined (Table 2) (Moutder et al., 1992), carbon (C) should originate from protein, wax or phenolic compounds, oxygen (O) from hydroxyl groups and the oxidation of sulphur, and sulphur (S) from amino acids. However, the origins of the silicon (Si) and calcium (Ca) was unclear from the experimental data. Ca found in *C. maculata* and *M. hebes* did not originate from the preservative as it was also detected in the fresh specimens of *T. jinpingensis*. The main chemical components should be wax or phenolic compounds because of the large proportion of atomic C and the small amount of Ca and other elements (N, O, S, Si; Table 2).

Therefore, the main reason for hydrophobicity is the tanned cuticulin in the cortex layer, which has a very strong adsorption to polar groups of the long chain hydrocarbons in the wax layer. This results in the orientation of the wax layer (monolayer) immediately above the cuticulin layer, so the nonpolar end of the long chain monolayer orients toward the outside. When the wing surfaces of five species (*C. maculate*, *M. hebes*, *P. scitula*, *M. conica* and *M. mongolica*) were cleaned with a writing brush, the nonpolar end of the orientated wax layer was removed and resulted in smaller contact angles than those cleaned only under flowing water (supplementary material Table S3), thus the surfaces becoming hydrophilic. This shows the wax layer plays an important role in hydrophobicity.

Relationship between SA and CA hysteresis

The SA was related to the weight of water droplets and the samples. When the drop was less than 3 μl, the weight was insufficient to overcome the energy barriers required to stick to all wing surfaces. When the drops were larger than 3 μl (on surface types C and D), the water droplets sliding a short distance were on the verge of rolling off the surfaces. The high SA values (Fig. 3; supplementary material Fig. S1) recorded after the drops re-pinned to the surfaces showed a significant CA hysteresis owing to a very large surface roughness (Youngblood and McCarthy, 1999; Lafuma and Quéré, 2003) resulting in high energy barriers (Nosonovsky, 2007b). Furthermore, the falling water droplets were captured by the wing veins before the three-phase line of contact moved resulting in a greater contact angle hysteresis. In addition, the compound contact state was very unstable because of its high roughness (Quéré and Reyssat, 2008). When transforming into the Wenzel state, it is more difficult for a small water droplet to roll off the surface and thus conquer higher energy barriers existing within the whole system; so the SA is high. When a droplet of water was greater than 7 μl, the effect of CA hysteresis was avoided (Wagner et al., 1996). Placing a water drop of 20 μl on the surface of *T. vacua*, resulted in the droplet sliding off when the wing was inclined at an angle of approximately 46 deg. Increasing the water volume to 30 μl resulted in the droplet sliding off at a smaller inclination (~26 deg.). Replicated surfaces mimicking structures of similar dimensions to the samples in our study have shown low hysteresis, suggesting a self-cleaning function (Watson et al., 2008).

Relationship between biology and wetting properties

Non-wetting surfaces offer survival value to terrestrial insects as they afford resistance to wetting by rain and other liquid surfaces they may encounter. Thus, there is a survival pay-off for such insects to adopt hydrophobic technologies especially on large surface areas such as wings.

Because of their low Reynolds values, additional weight on the wing resulting from contamination can potentially have a detrimental effect on flight. Small cicadas have the ability to clean their wings using extremities unlike large cicadas whose extremities are too short to completely extend over the entire wing. A variety of microstructured arrays on wing surfaces are the result of an evolutionary process for protection against wetting and contamination (Wagner et al., 1996), and are attributed to the biological adaptation and a special biofunction in the corresponding environment. Small and middle sized cicadas (types A and B in Fig. 1) generally live in shrubs and trees (often low in the tree canopy), where the leaf cover is large enough to shield the insect from rainwater. The larger cicadas (types C and D in Fig. 1) generally live high in trees where there is a more open environment of reduced leaf cover. This feature may be partly responsible for hydrophobicity variations. The general hydrophobic nature of the cicada wings may also aid in keeping the anti-reflective nature of the wing surface clean. Contamination of the anti-reflective coating by water, excrement or particulates would most likely degrade the optical properties of the wing membrane (e.g. a thin liquid layer would act as the first interface for reflecting light, while particulate contamination would cause diffuse scattering). A fully optimised anti-reflectance wing would presumably reduce losses from predators, thus maximising the mating opportunities and likelihood of procreation of the adult cicada.

Conclusions

Our experiments showed significantly different wettabilities of cicada forewings associated with distinct differences in surface patterning of nanostructures and their chemical components (wax

layer). When the wax on the wing membrane cuticle is intact, the specific architecture of nanostructuring will determine the hydrophobicity of wing surfaces. If the wax layer is removed then the hydrophobic surfaces will become hydrophilic.

Specimens with a larger diameter, closer spacing and greater height of protrusions generally exhibited stronger hydrophobic properties. The relative ratios of these parameters can also be used to predict the hydrophobicity of the surfaces. Arrangements of nanostructures which resulted in more disordered and inhomogeneous surfaces tended to exhibit lower contact angles. Thus surface 'defects' may perform a significant role in determining the wetting properties of these types of surfaces.

Although smaller water droplets were typically pinned to the surfaces, larger droplets showed reduced sliding angles. The roughness factor of the surfaces also played a role in the magnitude of CA hysteresis.

It is not clear how the wettability varies with developmental stage (how long after cicada nymph emerges from the ground), and this should be investigated in the near future using samples of various ages, and correlating these results with insect habit/behaviour.

The general observations and outcomes of our study may contribute to the understanding of how other insect species (terrestrial and semi-aquatic) minimise interactions with water.

LIST OF ABBREVIATIONS

φ	the solid fraction in contact with the liquid in the Cassie model
θ_A	advancing angle
θ_C	apparent contact angle on rough surface in the Cassie model
θ_O	contact angle on the flat surface of some material
θ_R	receding angle
θ_W	apparent contact angle on rough surface in the Wenzel model
a.c.	atom content
b.e.	binding energy
CA	contact angle
H	height of protrusion
L	spacing between of protrusions
r	the roughness factor (the ratio of actual area to the geometrically projected area of the surface) in Wenzel's model
R	diameter of protrusion
SA	sliding angle
v.s.	valence state of element

We thank Professor Jiang Lei for his assistance in the laboratory and for use of experimental instruments in the Institute of Chemistry, Chinese Academy of Sciences, and Dr Qudsia Tahseen for help in the preparation of the manuscript. This work is supported by the National Natural Science Foundation of China (grant numbers 30530110, 20571077), an Innovation Project of the Institute of Zoology of the Chinese Academy of Sciences, the National Science Fund for Fostering Talents in Basic Research (NSFC-J0030092), the Nation Research Fund for Fundamental Key Project (2007CB936403) and the Fund of Research Key Project (06311J2273).

REFERENCES

Barthlott, W. and Neinhuis, C. (1997). Purity of the sacred lotus, or escape from contamination in biological surfaces. *Planta* **202**, 1-8.
Bico, J., Thiele, U. and Quéré, D. (2002). Wetting of textured surfaces. *Colloids Surf. A* **206**, 41-46.
Bormashenko, E. (2008). Why does the Cassie-Baxter equation apply? *Colloids Surf. A* **324**, 47-50.
Cassie, A. B. D. and Baxter, S. (1944). Wettability of porous surfaces. *Trans. Faraday Soc.* **40**, 546-551.
Chapman, R. F. (1998). *The Insects: Structure and Function*. 4th edn. Cambridge: Cambridge University Press.
Chen, W., Fadeev, A. Y., Hsieh, M. C., Öner, D., Youngblood, J. and McCarthy, T. J. (1999). Ultrahydrophobic and ultralyophobic surfaces: some comments and examples. *Langmuir* **15**, 3395-3399.
Cong, Q., Chen, G., Fang, Y. and Ren, L. (2004). Super-hydrophobic characteristics of butterfly wing surface. *J. Bionic Eng.* **1**, 249-255.
Extrand, C. W. (2004). Criteria for ultralyophobic surfaces. *Langmuir* **20**, 5013-5018.
Fang, Y., Sun, G., Wang, T. Q., Cong, Q. and Ren, L. Q. (2007). Effect of non-smooth scale on surface wettability of butterfly wings. *J. Jilin Univ. (Eng. Tech. Ed.)* **37**, 582-586.
Feng, X. and Jiang, L. (2006). Design and creation of superwetting/antiwetting surfaces. *Adv. Mater.* **18**, 3063-3078.
Feng, X. Q., Gao, X., Wu, Z., Jiang, L. and Zheng, Q. S. (2007). Superior water repellency of water strider legs with hierarchical structures: experiments and analysis. *Langmuir* **23**, 4892-4896.
Gao, L. and McCarthy, T. J. (2007). How Wenzel and Cassie were wrong. *Langmuir* **23**, 3762-3765.
Gao, X. and Jiang, L. (2004). Water-repellent legs of water striders. *Nature* **432**, 36.
Goodwyn, P. P., De Souza, E., Fujisaki, K. and Gorb, S. (2008). Moulding technique demonstrates the contribution of suface goemetry to the super-hydrophobic properties of the surface of a water strider. *Acta Biomater.* **4**, 766-770.
Holdgate, M. W. (1955). The wetting of insect cuticles by water. *J. Exp. Biol.* **2**, 591-617.
Hsieh, C. T., Chen, J. M., Kuo, R. R., Lin, T. S. and Wu, C. F. (2005). Influence of surface roughness on water- and oil-repellent surfaces coated with nanoparticles. *Appl. Surf. Sci.* **240**, 318-326.
Jiang, L., Zhao, Y. and Zhai, J. (2004). A lotus-leaf-like superhydrophobic surface: a porous microsphere/nanofiber composite film prepared by electrohydrodynamics. *Angew. Chem. Int. Ed. Engl.* **43**, 4338-4341.
Jin, M., Feng, X., Feng, L., Sun, T., Zhai, J., Li, T. and Jiang, L. (2005). Superhydrophobic aligned polystyrene nanotube films with high adhesive force. *Adv. Mater.* **17**, 1977-1981.
Lafuma, A. and Quéré, D. (2003). Superhydrophobic states. *Nat. Mater.* **2**, 457-460.
Marmur, A. and Bittoun, E. (2009). When Wenzel and Cassie are right: reconciling local and global considerations. *Langmuir* **25**, 1277-1281.
Martines, E., Seunarine, K., Morgan, H., Gadegaard, N., Wilkinson, C. D. W. and Riehle, M. O. (2005). Superhydrophobicity and super-hydrophilicity of regular nanopatterns. *Nano Lett.* **5**, 2097-2103.
McHale, G. (2007). Cassie and Wenzel: were they really so wrong? *Langmuir* **23**, 8200-8205.
Ming, W., Wu, D., Van Benthem, R. and De With, G. (2005). Superhydrophobic films from raspberry-like particles. *Nano Lett.* **5**, 2298-2301.
Miwa, M., Nakajima, A., Fujishima, A., Hashimoto, K. and Watanabe, T. (2000). Effects of the surface roughness on sliding angles of water droplets on superhydrophobic surfaces. *Langmuir* **16**, 5754-5760.
Moutder, J. F., Stickie, W. F., Sobol, P. E. and Bomben, K. D. (1992). *Handbook of X-ray Photoelectron Spectroscopy* (ed. J. Chastain). Waltham, MA: Perkin-Elmer.
Nakajima, A., Fujishima, A., Hashimoto, K. and Watanabe, T. (1999). Preparation of transparent superhydrophobic boehmite and silica films by sublimation of aluminum acetylacetonate. *Adv. Mater.* **11**, 1365-1368.
Neinhuis, C. and Barthlott, W. (1997). Characterization and distribution of water-repellent, self-cleaning plant surfaces. *Ann. Bot.* **79**, 667-677.
Nishino, T., Meguro, M., Nakamae, K., Matsushita, M. and Ueda, Y. (1999). The lowest surface free energy based on -CF_3 alignment. *Langmuir* **15**, 4321-4323.
Nosonovsky, M. (2007a). On the range of applicability of the Wenzel and Cassie equations. *Langmuir* **23**, 9919-9920.
Nosonovsky, M. (2007b). Multiscale roughness and stability of superhydrophobic biomimetic interfaces. *Langmuir* **23**, 3157-3161.
Öner, D. and McCarthy, T. J. (2000). Ultrahydrophobic surfaces. Effects of topography length scales on wettability. *Langmuir* **16**, 7777-7782.
Panchagnula, M. V. and Vedantam, S. (2007). Comment on how Wenzel and Cassie were wrong by Gao and McCarthy. *Langmuir* **23**, 13242-13242.
Patankar, N. A. (2004). Mimicking the lotus effect: influence of double roughness structures and slender pillars. *Langmuir* **20**, 8209-8213.
Quéré, D. and Reyssat, M. (2008). Non-adhesive lotus and other hydrophobic materials. *Philos. Transact. A Math. Phys. Eng. Sci.* **366**, 1539-1556.
Shi, F., Wang, Z. and Zhang, X. (2005). Combining a layer-by-layer assembling technique with electrochemical deposition of gold aggregates to mimic the legs of water striders. *Adv. Mater.* **17**, 1005-1009.
Shiu, J. Y., Kuo, C. W., Chen, P. L. and Mou, C. Y. (2004). Fabrication of tunable superhydrophobic surfaces by nanosphere lithography. *Chem. Mater.* **16**, 561-564.
Song, F., Lee, K. L., Soh, A. K., Zhu, F. and Bai, Y. L. (2004). Experimental studies of the material properties of the forewing of cicada (Homoptera, Cicadidae). *J. Exp. Biol.* **207**, 3035-3042.
Stoddart, P. R., Cadusch, P. J., Boyce, T. M., Erasmus, R. M. and Comins, J. D. (2006). Optical properties of chitin: surface-enhanced Raman scattering substrates based on antireflection structures on cicada wings. *Nanotechnology* **17**, 680-686.
Sun, T., Feng, L., Gao, X. and Jiang, L. (2005). Bioinspired surfaces with special wettability. *Acc. Chem. Res.* **38**, 644-652.
Wagner, T., Neinhuis, C. and Barthlott, W. (1996). Wettability and contaminability of insect wings as a function of their surface sculptures. *Acta Zool. (Stockholm)* **77**, 213-225.
Watson, G. S. and Watson, J. A. (2004). Natural nano-structures on insects – possible functions of ordered arrays characterized by atomic force microscopy. *Appl. Surf. Sci.* **235**, 139-144.
Watson, G. S., Myhra, S., Cribb, B. W. and Watson, J. A. (2008). Putative functions and functional efficiency of ordered cuticular nanoarrays on insect wings. *Biophys. J.* **94**, 3352-3360.
Wenzel, R. N. (1936). Resistance of solid surfaces to wetting by water. *Ind. Eng. Chem. Res.* **28**, 988-994.
Xie, Q., Xu, J., Feng, L., Jiang, L., Tang, W., Luo, X. and Han, C. C. (2004). Facile creation of a super-amphiphobic coating surface with bionic microstructure. *Adv. Mater.* **16**, 302-305.
Youngblood, J. P. and McCarthy, T. J. (1999). Ultrahydrophobic polymer surfaces prepared by simultaneous ablation of polypropylene and sputtering of poly (tetrafluoroethylene) using radio frequency plasma. *Macromolecules* **32**, 6800-6806.
Zhang, G., Zhang, J., Xie, G., Liu, Z. and Shao, H. (2006). Cicada wings: a stamp from nature for nanoimprint lithography. *Small* **2**, 1440-1443.
Zhang, X., Lou, S., Zhang, X., Sun, J. and Hu, J. (2003). Studies on nanobubbles formed at solid/liquid interface. *J. Chin. Electr. Microsc. Soc.* **22**, 136-141.
Zheng, L. J., Wu, X. D., Lou, Z. and Wu, D. (2004). Preparation of the micro-structured super-hydrophobic surface. *Chin. Sci. Bull.* **49**, 1691-1699.

Figure S1. The contact angles (CA) and sliding angle (SA) on cicada wings

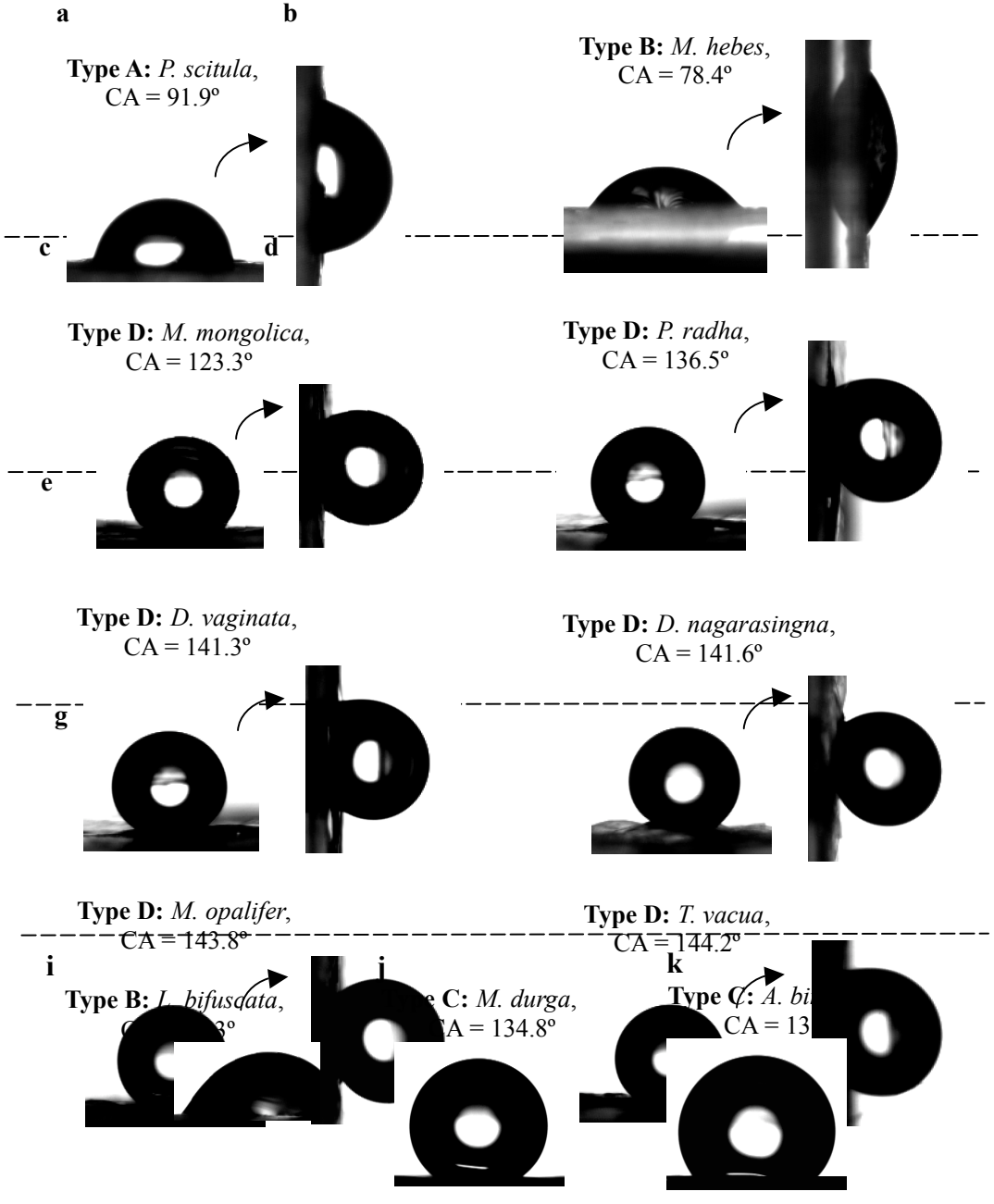

Figure S2. XPS analysis on wings of four cicada species

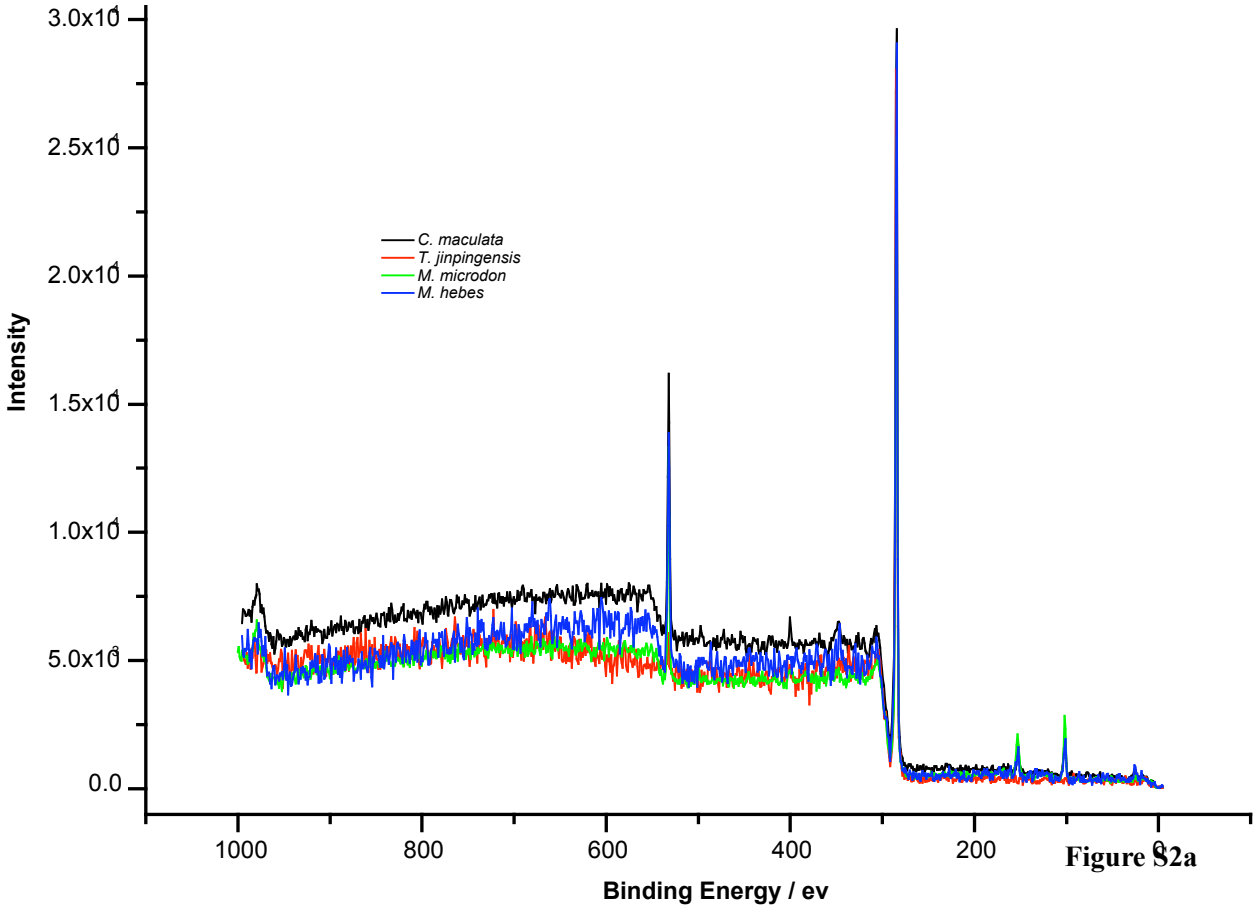

Figure S2a

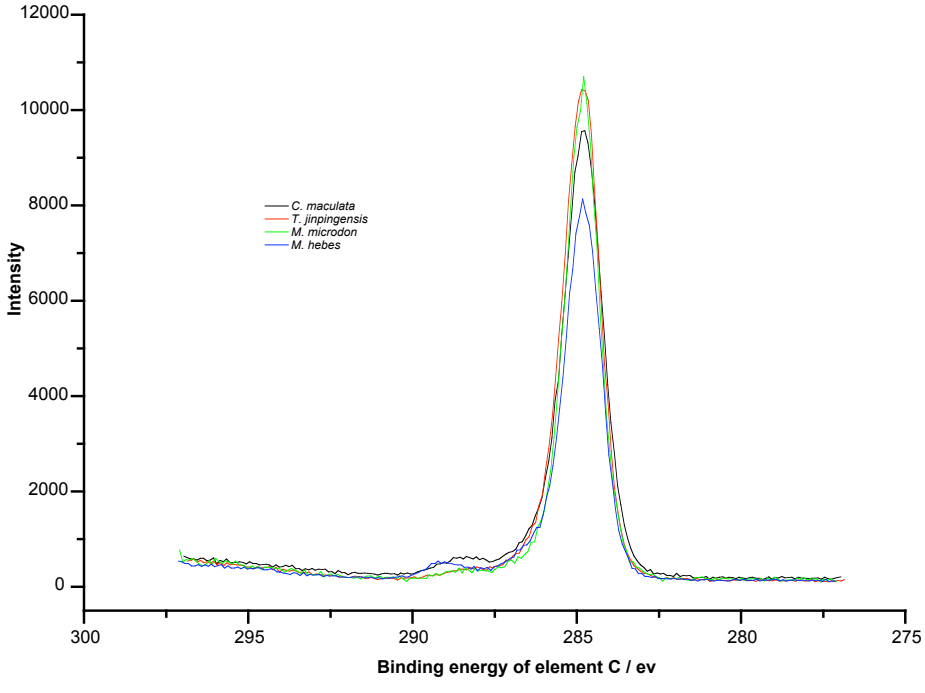

Figure S2b

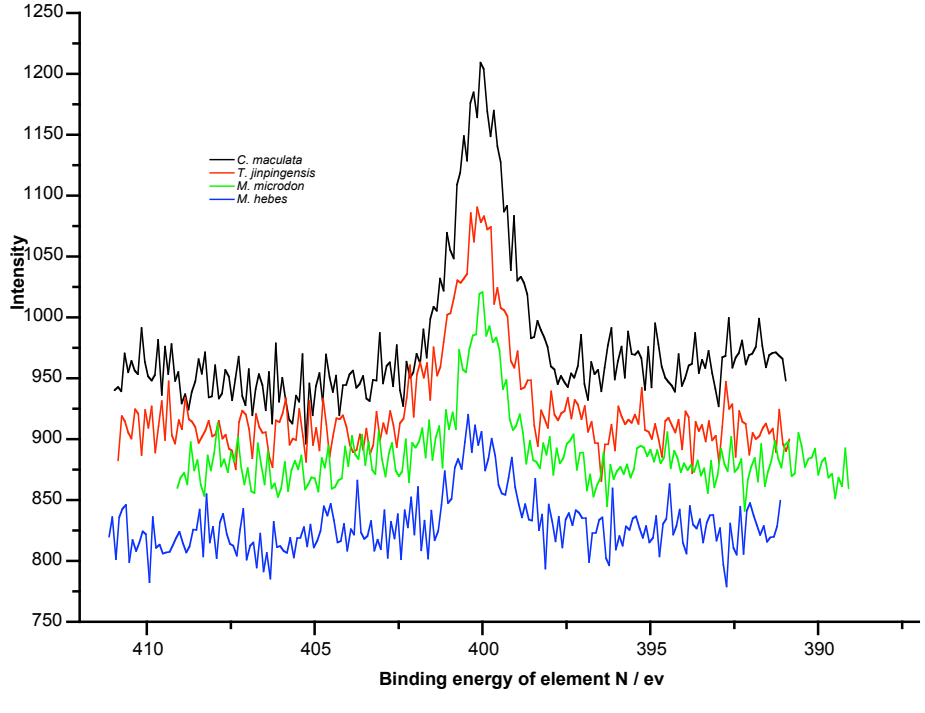

Figure S2c

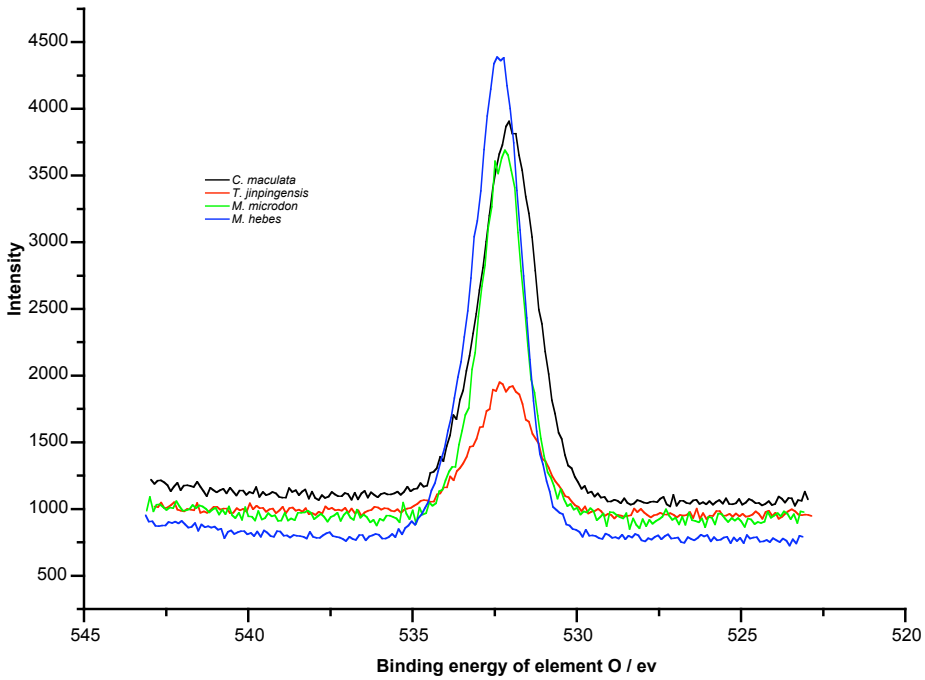

Figure S2d

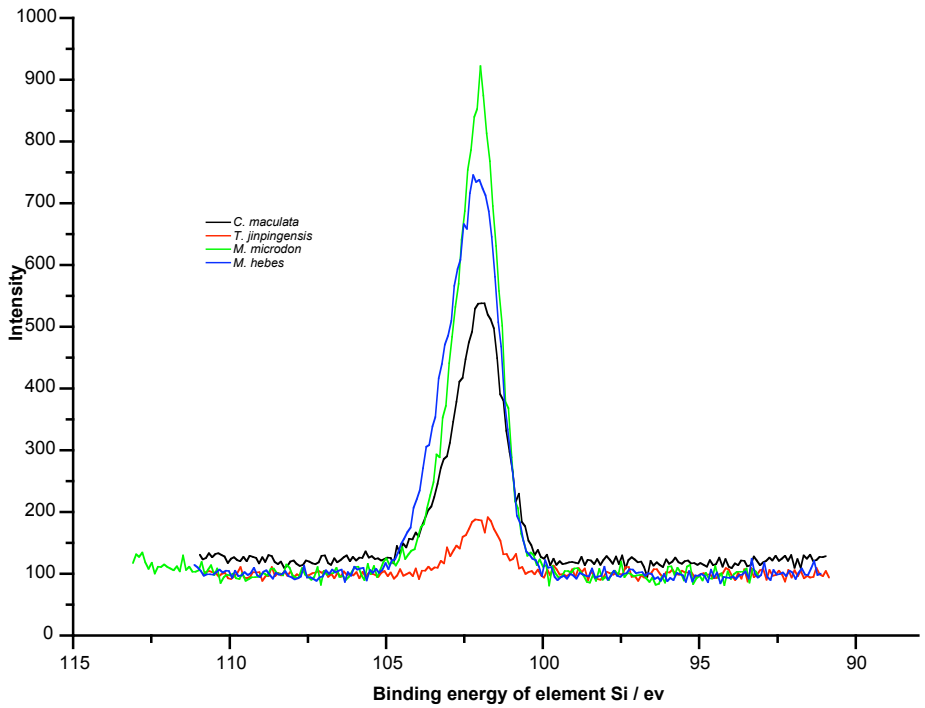

Figure S2e

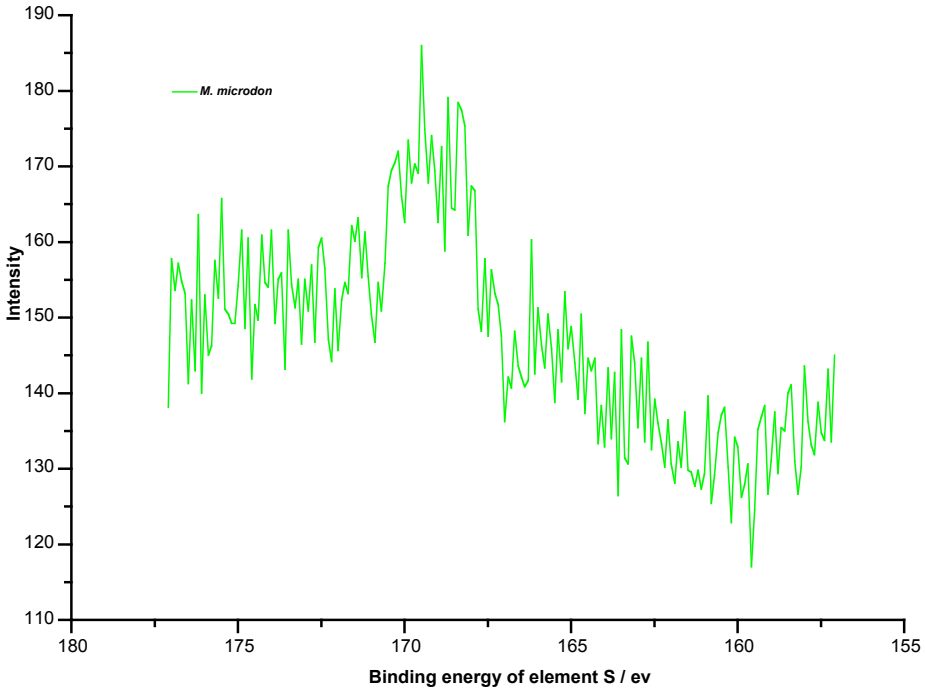

Figure S2f

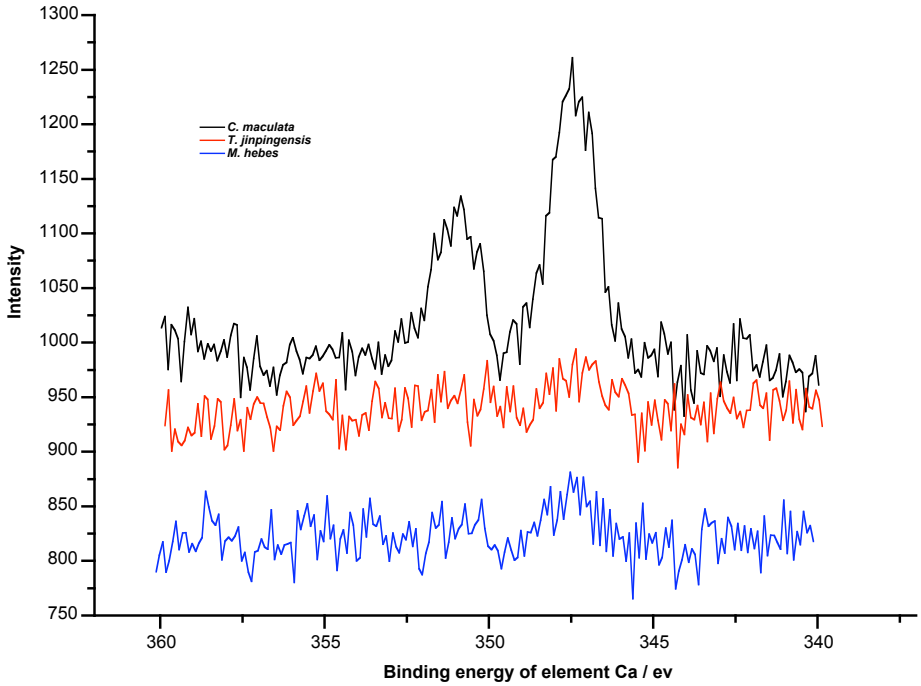

Figure S2g

Table S1. Ratio of diameter (*R*), spacing (*L*) and height (*H*) of protrusions and values of roughness factor (*r*), solid fraction in contact with the liquid (φ), $\cos\theta_w$ and $\cos\theta_c$ based on the Wenzel and Cassie models (standard deviations in brackets)

			Ratio		Wenzel model		Cassie model	
Type	Species	CA (deg.)	*H/L*	*L/R*	*r*	$\cos\theta_w$	φ	$\cos\theta_c$
A	*C. maculate*	76.8 (13.9)	3.37	0.95	4.37	–1.13	0.263	–0.805
	P. scitula	91.9 (5.9)	3.36	1.00	4.36	–1.13	0.250	–0.815
B	*M. hebes*	78.4 (5.0)	1.73	1.12	2.72	–0.704	0.223	–0.835
	L. bifuscata	81.3 (8.3)	1.71	1.30	2.68	–0.259	0.189	–0.860
	M. conica	93.9 (8.3)	1.37	1.21	2.36	–0.611	0.205	–0.848
C	*M. durga*	134.8 (5.7)	2.89	1.00	3.82	–0.989	0.250	–0.815
	A. bindusara	135.5 (5.2)	2.57	1.08	3.57	–0.923	0.230	–0.829
	M. microdon	139.8 (4.5)	2.34	1.09	3.33	–0.863	0.230	–0.830
D	*M. mongolica*	123.3 (12.7)	8.85	0.37	7.95	–2.06	0.535	–0.604
	P. radha	136.5 (5.2)	6.55	0.32	5.82	–1.51	0.573	–0.575
	D. vaginata	141.3 (3.3)	6.46	0.42	6.41	–1.66	0.493	–0.635
	D. nagarasingna	141.6 (4.5)	6.72	0.37	6.28	–1.63	0.535	–0.604
	M. opalifer	143.8 (6.0)	8.71	0.32	7.44	–1.93	0.570	–0.577
	T. vacua	144.2 (6.8)	10.14	0.31	8.35	–2.16	0.581	–0.570
	T. jinpingensis	146.0 (2.6)	8.52	0.33	7.32	–1.90	0.569	–0.579

CA, contact angles (standard deviations in brackets).

Table S2. Advancing (θ_A) and receding angles (θ_R) of wing surfaces of five cicada species

Type	Species	θ_A (deg.)	θ_R (deg.)	Hystersis
B	*M. conica*	79.5	73.3	6.2
C	*A. bindusara*	139.6	138.6	1.0
	D. vaginata	141.2	139.1	2.1
D	*D. nagarasingna*	140.6	139.7	0.9
	T. vacua	145.1	144.4	0.7

Table S3. Mean contact angles (standard deviations in brackets) of wing surfaces of five cicada species, cleaned with flowing deionized water or cleaned with deionized water and a fine brush

	Measured contact angles of wing surface (deg.)	
Species	Cleaned with deionized water	Cleaned with deionized water and a fine brush
C. maculata	76.8 (13.9)	70.5 (4.3)
M. hebes	78.4 (5.0)	61.0 (3.2)
P. scitula	91.9 (5.9)	66.1 (10.0)
M. conica	93.9 (8.3)	75.7 (3.0)
M. mongolica	123.3 (12.7)	75.6 (11.5)